Comp. Appl. Math. (2016) 35:881–891
DOI 10.1007/s40314-015-0295-3

On retrograde orbits, resonances and stability

M. H. M. Morais[1] · **F. Namouni**[2]

Received: 15 April 2015 / Revised: 12 October 2015 / Accepted: 1 November 2015 /
Published online: 20 November 2015

Abstract We start by reviewing our previous work on retrograde orbital configurations and on modeling and identifying retrograde resonances. Then, we present new results regarding the enhanced stability of retrograde configurations with respect to prograde configurations in the low mass ratio regime of the planar circular restricted 3-body problem. Motivated by the recent discovery of small bodies which are in retrograde resonance with the Solar System's giant planets we then explore the case with mass ratio 0.001 and show new stability maps in a grid of semi-major axis versus eccentricity for the 2/1 and 1/2 retrograde resonances. Finally, we explain how the stability borders of the 2/1 and 1/2 retrograde resonances are related to the resonant orbits' geometry.

Keywords Resonance · Stability · Retrograde

Mathematics Subject Classification 70F15 · 70F07

1 Introduction

A retrograde orbital configuration consists of two or more bodies moving around a central mass in opposite directions or, more precisely, such that the relative inclination[1] $180° \geq I > 90°$. When $I = 180°$ the orbits are retrograde and coplanar.

[1] The relative inclination between two orbits is the angle between the respective angular momentum vectors.

Communicated by Elbert E. N. Macau, Antônio Fernando Bertachini de Almeida Prado and Cristiano Fiorilo de Melo.

✉ M. H. M. Morais
helena.morais@gmail.com; helena.morais@rc.unesp.br

[1] Instituto de Geociências e Ciências Exatas, Universidade Estadual Paulista (UNESP), Av. 24-A, 1515, 13506-900 Rio Claro, SP, Brazil

[2] Université de Nice, CNRS, Observatoire de la Côte dAzur, CS 34229, 06304 Nice, France

Examples of retrograde orbital motion in the Solar System include: many comets, 63 small bodies[2] including Mars crossing asteroids, a subset of Centaurs called Damocloids, a TNO (2008KV42), and distant objects on nearly parabolic orbits. Many irregular satellites of the giant planets and Neptune's moon Triton also have retrograde orbital motion. Extrasolar planetary systems are detected through indirect methods and the relative inclinations are usually not known.[3] Retrograde configurations could be achieved, e.g., through capture of a free-floating planet in a star cluster which has isotropic probability (Perets and Kouwenhoven 2012; Varvoglis et al. 2012).

Analysis of radial velocity data for the star ν-Octantis A by Ramm et al. (2009) led to the claim that there is a planet about half-way between ν-Octantis A and its binary companion, ν-Octantis B. This result was puzzling since a planet at such location in a prograde configuration would be unstable due to the strong perturbation from ν-Octantis B and led to alternative hypothesis for this system (Morais and Correia 2012). Numerical integrations by Eberle and Cuntz (2010) and Goździewski et al. (2013) showed that a planet in a retrograde configuration could be stable in the ν-Octantis system which prompted a study of the stability of retrograde configurations in binary systems by Morais and Giuppone (2012). This showed that the enhanced stability of retrograde configurations with respect to prograde configurations is due to the nature of retrograde resonances which are weaker than prograde resonances at a given orbital period ratio (Morais and Giuppone 2012).

Morais and Namouni (2013) studied retrograde resonance in the framework of the circular restricted 3-body problem (CR3BP), identifying the relevant resonant arguments in the disturbing function and exploring retrograde resonance stability using the method of surfaces of section. Morais and Namouni (2013) identified small bodies (Damocloids) which are currently in the 1/2 and 2/5 retrograde resonances with Jupiter, and in the 2/3 retrograde resonance with Saturn. In Namouni and Morais (2015) we performed a numerical study of the resonance capture probabilities for objects on prograde and retrograde orbits migrating inwards towards a Jupiter mass planet. We saw that capture in resonance is more likely for retrograde inclinations ($I > 90°$) rather than prograde inclinations ($I < 90°$).

This article is organized as follows. In Sect. 2 we review our work on the retrograde disturbing function, explain how to obtain retrograde resonance's critical angles and associated resonance strength. In Sect. 3, we present results on the enhanced stability of retrograde configurations with respect to prograde configurations for mass ratio <0.01 relevant for planetary systems. In Sect. 4 we show stability maps in a grid of semi-major axis versus eccentricity for the 2/1 and 1/2 retrograde resonances. In Sect. 5 we discuss our results.

2 Retrograde resonance

2.1 Retrograde and prograde disturbing functions

Consider the restricted 3-body problem consisting of a test particle subject to the gravitational influence of a primary and secondary (mass ratio μ) which move on a circular orbit of unit radius (CR3BP). The disturbing function is[4]

[2] Listed on http://www.minorplanetcenter.net/on10/4/2015.

[3] The radial velocity method usually does not constrain relative inclinations while the transit method only allows to detect nearly aligned systems.

[4] We use standard Keplerian elements for the test particle's orbit: a (semi-major axis), e (eccentricity), I (inclination), f (true anomaly), ω (argument of pericenter), Ω (longitude of ascending node), λ (mean longitude). The secondary's circular orbit has semi-major axis $a' = 1$ and mean longitude λ'.

$$R = \mu \left(\frac{1}{\Delta} - r \cos \psi \right) \tag{1}$$

where r is the radial distance to the primary, $\Delta = \sqrt{1 + r^2 - 2r\ \cos \psi}$,

$$\begin{aligned} \cos \psi &= \cos(f + \omega) \cos(\Omega - \lambda') - \sin(f + \omega) \sin(\Omega - \lambda') \cos I \\ &= \cos^2(I/2) \cos(f + \omega + \Omega - \lambda') + \sin^2(I/2) \cos(f + \omega - \Omega + \lambda') \,. \end{aligned} \tag{2}$$

If the orbit is prograde with inclination $I \approx 0$ then $\sin^2(I/2) \ll 1$, hence we define a small parameter

$$\Psi = \cos \psi - \cos(f + \omega + \Omega - \lambda') = 2\ \sin^2(I/2) \sin(\Omega - \lambda') \sin(\omega + f), \tag{3}$$

and expanding the direct term of Eq. (1) around $\Psi = 0$ leads to the classical expression (Murray and Dermott 1999)

$$\frac{1}{\Delta} = \sum_{i=0}^{\infty} \frac{(2i)!}{(i!)^2} \left(\frac{1}{2} r \Psi \right)^i \frac{1}{\Delta_0^{2\,i+1}} \tag{4}$$

with $\Delta_0 = \sqrt{1 + r^2 - 2r\ \cos(f + \omega + \Omega - \lambda')}$.

If the orbit is retrograde with inclination $I \approx 180°$ then $\cos^2(I/2) \ll 1$, hence $\Psi \gg 1$ and the expansion in Eq. 4 is not valid. Following Morais and Namouni (2013) we define a small parameter

$$\bar{\Psi} = \cos \psi - \cos(f + \omega - \Omega + \lambda') = 2\ \cos^2(I/2) \sin(-\Omega + \lambda') \sin(\omega + f), \tag{5}$$

and expanding the direct term of Eq. (1) around $\bar{\Psi} = 0$ leads to

$$\frac{1}{\Delta} = \sum_{i=0}^{\infty} \frac{(2i)!}{(i!)^2} \left(\frac{1}{2} r \bar{\Psi} \right)^i \frac{1}{\bar{\Delta}_0^{2\,i+1}} \tag{6}$$

with $\bar{\Delta}_0 = \sqrt{1 + r^2 - 2r\ \cos(f + \omega - \Omega + \lambda')}$.

Therefore, we see that the expansions of the disturbing function for prograde (Eq. 4) and retrograde (Eq. 6) orbits are related. The latter may be obtained from the former by performing the following canonical transformation (Morais and Namouni 2013)

$$I^\star = 180° - I \quad \lambda'^\star = -\lambda' \quad \omega^\star = \omega - \pi \quad \Omega^\star = -\Omega - \pi. \tag{7}$$

The canonical transformation (Eq. 7) has a physical meaning: it is analogous to obtaining a retrograde orbit of inclination I from a prograde orbit of inclination $180° - I$ by simply inverting the motion of the massive bodies. This is the 3D version of the procedure described in Morais and Giuppone (2012) to obtain the retrograde disturbing function from the prograde disturbing function in the planar (2D) problem.

2.2 Retrograde resonance critical angles

By inspection of the disturbing function's expansion (Eq. 6) we conclude that at the p/q retrograde resonance the slow terms are[5]

[5] The order of a retrograde p/q resonance is equal to $p + q$ which is the factor of the $\varpi^\star$ term in the resonant argument with $k = 0$ of the retrograde disturbing function (Morais and Namouni 2013). Conversely, the order of a prograde p/q resonance is equal to $p - q$ which is the factor of the ϖ term in the resonant argument with $k = 0$ of the prograde disturbing function (Murray and Dermott 1999).

$$e^{p+q-2k}\cos^{2k}(I/2)\cos(q\,\lambda^\star + p\,\lambda'^\star - (p+q-2k)\varpi^\star - 2k\,\Omega^\star) \tag{8}$$

with $2k \leq p+q$, $\lambda^\star = \lambda - 2\,\Omega$, $\varpi^\star = \omega - \Omega = \varpi - 2\,\Omega$.

As an example we discuss the case of the 2/1 and 1/2 resonances. The 2/1 (1/2) prograde resonance has critical angle $\lambda - 2\,\lambda' + \varpi$ ($2\,\lambda - \lambda' - \varpi$), which appears at 1st order in eccentricity, i.e. the amplitude (or strength) of the resonance term is $\mathcal{O}(e)$, while the 2/1 and 1/2 retrograde resonances have 2 critical angles each which appear at 3rd order in eccentricity and inclination. The 2/1 retrograde resonance has critical angles:

- $\phi^\star_{21} = \lambda^\star + 2\,\lambda'^\star - 3\,\varpi^\star = \lambda - 2\,\lambda' - 3\,\varpi + 4\,\Omega$, $\quad\mathcal{O}(e^3)$;
- $\phi^\star_{21} = \lambda^\star + 2\,\lambda'^\star - \varpi^\star - 2\,\Omega^\star = \lambda - 2\,\lambda' - \varpi + 2\,\Omega$, $\quad\mathcal{O}(e\cos^2(I/2))$;

while the 1/2 retrograde resonance has critical angles:

- $\phi^\star_{12} = 2\,\lambda^\star + \lambda'^\star - 3\,\varpi^\star = 2\,\lambda - \lambda' - 3\,\varpi + 2\,\Omega$ $\quad\mathcal{O}(e^3)$;
- $\phi^\star_{12} = 2\,\lambda^\star + \lambda'^\star - \varpi^\star - 2\,\Omega^\star = 2\,\lambda - \lambda' - \varpi$, $\quad\mathcal{O}(e\cos^2(I/2))$.

In the planar (2D) problem the 2/1 and 1/2 retrograde resonances have single critical angles, $\phi^\star_{21} = \lambda^\star - 2\,\lambda' - 3\,\varpi^\star$ and $\phi^\star_{12} = 2\,\lambda^\star - \lambda' - 3\,\varpi^\star$, respectively. Figure 1 shows planar orbits in the 2/1 retrograde resonance corresponding to libration of $\phi^\star_{21}$ around 0 or 180°. Figure 2 shows planar orbits in the 1/2 retrograde resonance corresponding to libration of $\phi^\star_{12}$ around 0 or 180°. The location of the resonances' centers at a given mass ratio μ depends on a and e as we will confirm in Sect. 4.

3 Enhanced stability of retrograde configurations

In Morais and Giuppone (2012) we showed that a planet orbiting the primary star of a binary may be stable closer to the secondary star if it has a retrograde orbit rather than a prograde orbit. We explained that this is due to retrograde resonances being weaker than prograde resonances, i.e., at a given mean motion ratio p/q, prograde resonances are of order $p-q$ while retrograde resonances are of order $p+q$. This has two effects on stability: (1) the excitation of eccentricity is smaller for retrograde resonances; (2) the overlap of resonances which generates a chaotic layer in the vicinity of the secondary (Wisdom 1980) is less widespread for retrograde configurations. This can also be understood in terms of the effect of close encounters with the secondary which generate the chaotic layer in its vicinity. Close encounters in retrograde configurations occur at larger relative velocity (hence have shorter duration and consequently are less disruptive to the orbit) than in prograde configurations.

Morais and Giuppone (2012) were interested in the high mass ratio regime and inner orbits, relevant for studying the stability of a planet around the primary star of a binary system. Here, we revisit the problem of stability concentrating in the low mass ratio regime ($\mu < 0.01$) and both inner and outer orbits. This is relevant for a small body (test particle) orbiting a star subject to the perturbation by a nearby planet (mass ratio μ). We numerically integrate the equations of motion of the CR3BP, together with the variational equations and MEGNO[6] equations (Cincotta and Simó 2000; Goździewski 2003) for 5×10^4 binary's periods.

In Fig. 3 we show the MEGNO maps for retrograde (top panel) and prograde (low panel) configurations in a grid of semi-major axis $1.2 \geq a \geq 0.8$ varying at steps $0.05\,R_H$, and mass ratio $0.01 \geq \mu \geq 0.0001$ varying at steps 0.0001. The other initial orbital elements with respect to the primary were: $e = 0, \lambda = \lambda', \omega = 0, I = 180°$ (retrograde configuration)

[6] The fast chaos indicator MEGNO is an acronym for Mean Exponential Growth factor of Nearby Orbits.

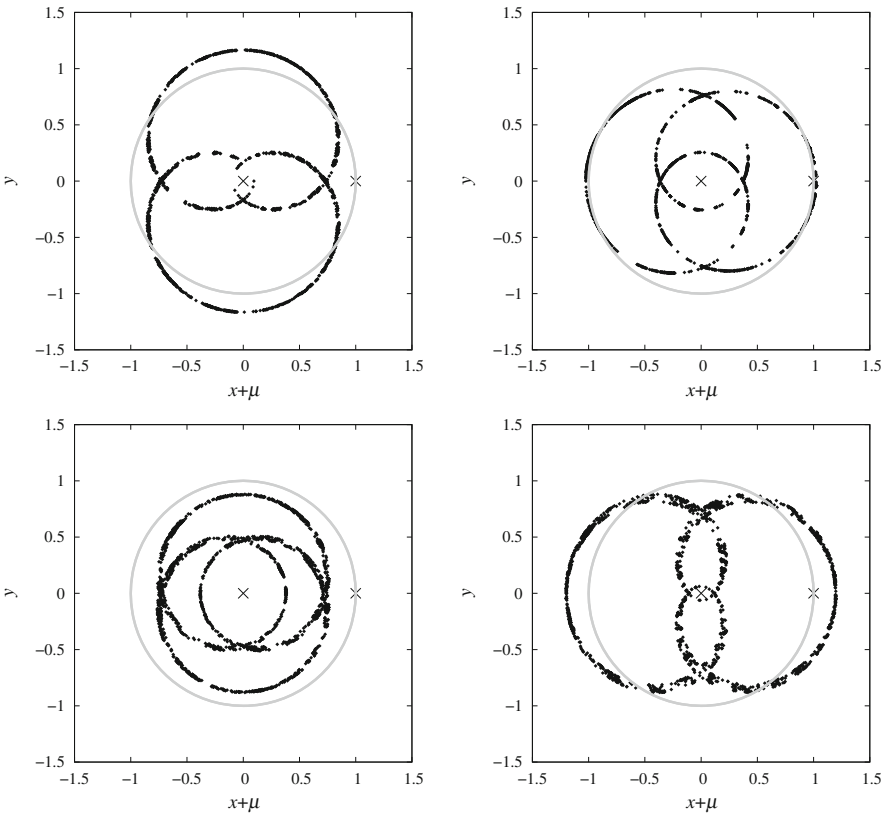

Fig. 1 Orbits in 2/1 retrograde resonance (CR3BP with mass ratio $\mu = 0.001$): libration around 0 (*left*) with $a = 0.63$ and $e = 0.8$ (*top*) or $e = 0.4$ (*low*); libration around 180° (*right*) with $a = 0.64$ and $e = 0.6$ (*top*) or $a = 0.63$ and $e = 0.9$ (*low*). The star and planet are identified by *symbol cross* at (0, 0) and (1, 0) and the *gray circle* has unit radius

or $I = 0$ (prograde configuration). The mean MEGNO $\langle Y \rangle$ converges to 2 for regular orbits and increases at a rate inversely proportional to Lyapunov's time for chaotic orbits (Cincotta and Simó 2000; Goździewski 2003). We set the maximum $\langle Y \rangle$ value for chaotic orbits as 8 to have a high contrast between the regular (blue) and chaotic (yellow) regions in Fig. 3.

Black dashed lines in Fig. 3 (low panel) approximate the region of first-order resonance's overlap for low mass ratio (width $1.33\,\mu^{2/7}$) known as Wisdom's stability criterion (Wisdom 1980). In Fig. 3 (low panel) we show only a zoom of the chaotic region with $0.8 \leq a \leq 1.2$ to compare with Fig. 3 (top panel). The boundary of Hill's region (width $R_H = (\mu/3)^{1/3}$) is marked by black solid lines in Fig. 3. We see that for prograde configurations, a thick chaotic layer always separates Hill's region from the inner and outer regular regions. This implies that smooth migration capture in the 1/1 prograde resonance is not possible for initial circular orbits outside Hill's region in agreement with our study of resonance capture (Namouni and Morais 2015). In contrast, for retrograde configurations, Hill's region connects to the inner and outer regular regions. Moreover, in Fig. 3 (top panel) there is striking asymmetry between the inner and outer stability boundaries, both contained within Hill's region. Indeed, the outer boundary has a stability island separating the internal chaotic region from an external chaotic

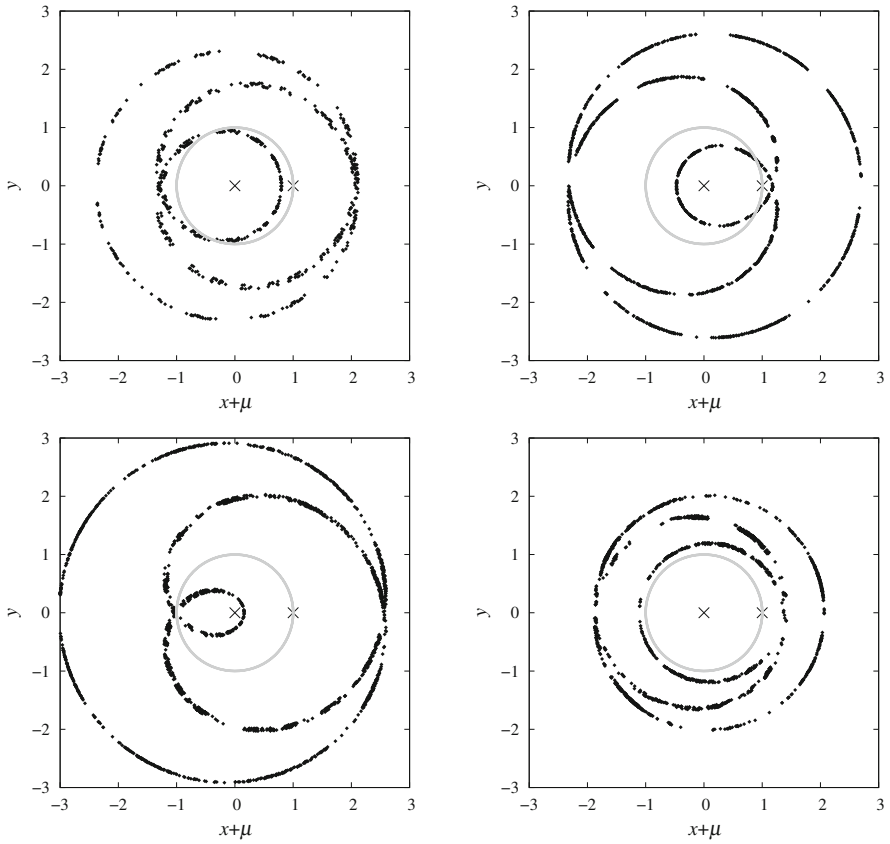

Fig. 2 Orbits in 1/2 retrograde resonance (CR3BP with mass ratio $\mu = 0.001$): libration around 0 (*left*) with $a = 1.6$ and $e = 0.5$ (*top*) or $a = 1.59$ and $e = 0.9$ (*low*); libration around 180° (*right*) with $a = 1.59$ and $e = 0.7$ (*top*) or $e = 0.3$ (*low*). The star and planet are identified by *symbol cross* at (0, 0) and (1, 0) and the *gray circle* has unit radius

strip. The orbits within the stability island are in the 1/1 retrograde resonance where the critical angle[7] $\phi_{11}^{\star} = \lambda - \lambda' - 2\,\omega$ librates around 0 with large amplitude (Fig. 4).

4 Stability maps of 2/1 and 1/2 retrograde resonances

As seen in Sect. 2.2 and Morais and Namouni (2013) the strongest retrograde resonance is the 1/1 (order 2), followed by the 2/1 and 1/2 (order 3). Here, we explore the stability of the 2/1 and 1/2 retrograde resonances, leaving a detailed study of the 1/1 retrograde resonance for a future publication. To that purpose we fix the mass ratio at $\mu = 0.001$ (which represents a small body in the Sun–Jupiter system) and numerically integrate the equations of motion of the CR3BP, together with the variational equations and MEGNO equations (Cincotta and Simó 2000; Goździewski 2003) for 5×10^4 binary's periods. As before, we set the maximum mean MEGNO $\langle Y \rangle$ value for chaotic orbits as 8 to have a high contrast between the regular (blue) and chaotic (yellow) regions.

[7] As seen in Morais and Namouni (2013) the critical angle of the 2D retrograde 1/1 resonance is $\lambda - \lambda' - 2\,\omega$.

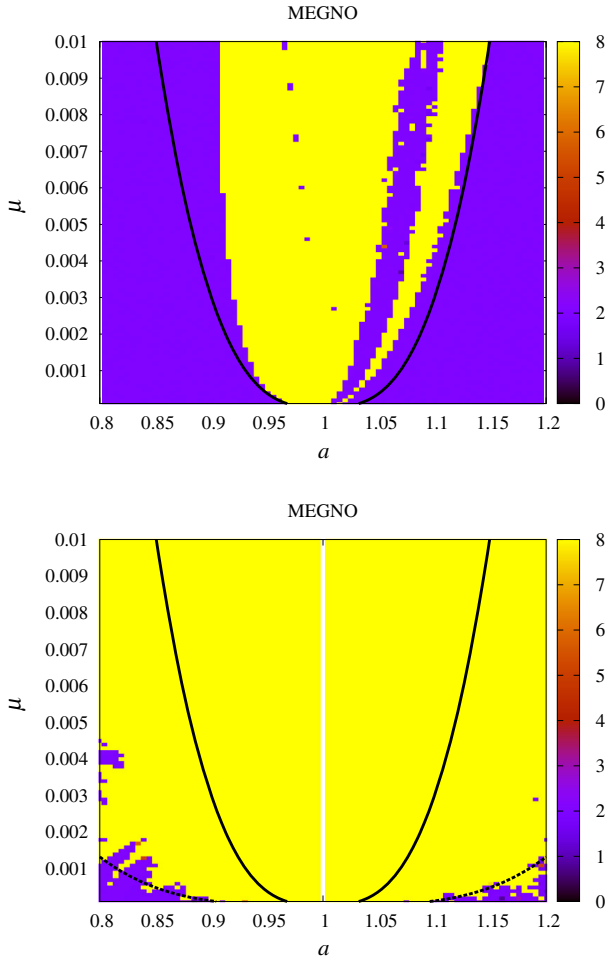

Fig. 3 Stability boundary between regular (*blue*) and chaotic (*yellow*) regions for initially circular orbits: retrograde configuration (*top panel*) and prograde configuration (*low panel*). *Black solid lines* show edge of Hill's region (width $(\mu/3)^{1/3}$) while *black dashed lines* show Wisdom's stability boundary (width $1.33\,\mu^{2/7}$). (Color figure online)

4.1 The 2/1 retrograde resonance

The test particle's initial conditions for the 2/1 retrograde resonance are: inclination $I = 180°$, semi-major axis in $(0.63 - 0.3\,R_H, 0.63 + 0.3\,R_H)$ varying at steps $0.01\,R_H$, eccentricity in $(0, 1)$ varying at steps 0.05, $\Omega = \omega = 0$, $\phi_{21}^\star = \lambda^\star - 2\,\lambda' - 3\,\varpi^\star = 0, 180°$, with $\lambda^\star = \lambda - 2\,\Omega$, $\varpi^\star = \omega - \Omega$. In Fig. 5 we show the MEGNO maps for configurations with $\phi_{21}^\star = 0$ (top panel) and $\phi_{21}^\star = 180°$ (low panel). The initial (a, e) corresponding to the orbits in Fig. 1 (left) are marked in Fig. 5 (top), while those corresponding to the orbits in Fig. 1 (right) are marked in Fig. 5 (low).

The 2/1 retrograde resonant mode with $\phi_{21}^\star$ librating around 0 has close approaches with the planet between pericenter and apocenter (Fig. 1, left) while the one with $\phi_{21}^\star$ librating around 180° has closest approaches with the planet at apocenter (Fig. 1, right). Hence, the

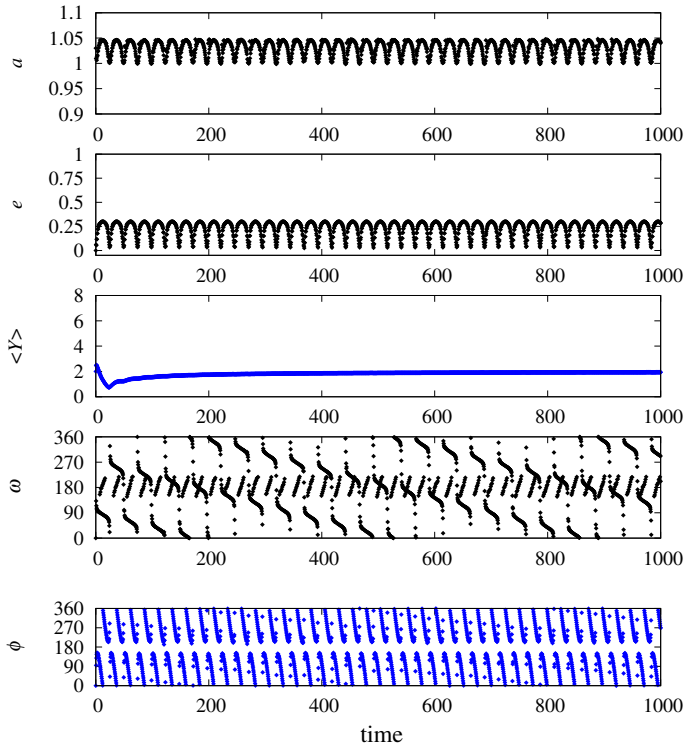

Fig. 4 Orbit within stability island of Fig. 3 (*top panel*) for mass ratio $\mu = 0.001$. *From top to bottom* semi-major axis a, eccentricity e, mean MEGNO $\langle Y \rangle$, argument of pericenter ω, critical angle of 2D retrograde 1/1 resonance $\phi = \lambda - \lambda' - 2\,\omega$

apocentric collision line (black) limits the border of the resonance in Fig. 5 (low panel). Libration in the resonance with center $\phi^{\star}_{21} = 180°$ is only possible above this collision line and the border is chaotic (yellow) except for a gap between $0.63 < a < 0.64$ connecting the regular resonant and non-resonant regions.

4.2 The 1/2 retrograde resonance

The test particle's initial conditions for the 1/2 retrograde resonance are: inclination $I = 180°$, semi-major axis in $(1.59 - 0.3\,R_H, 1.59 + 0.3\,R_H)$ varying at steps $0.01\,R_H$, eccentricity in $(0, 1)$ varying at steps 0.05, $\Omega = \omega = 0$, $\phi^{\star}_{12} = 2\,\lambda^{\star} - \lambda' - 3\,\varpi^{\star} = 0, 180°$, with $\lambda^{\star} = \lambda - 2\,\Omega$, $\varpi^{\star} = \omega - \Omega$. In Fig. 6 we show the MEGNO maps for configurations with $\phi^{\star}_{12} = 0$ (top panel) and $\phi^{\star}_{12} = 180°$ (low panel). The initial (a, e) corresponding to the orbits in Fig. 2 (left) are marked in Fig. 6 (top), while those corresponding to the orbits in Fig. 2 (right) are marked in Fig. 6 (low).

The 1/2 retrograde resonant mode with $\phi^{\star}_{12}$ librating around 0 has close approaches with the planet at pericenter (Fig. 2, left) while the one with $\phi^{\star}_{12}$ librating around 180° has closest approaches with planet between apocenter and pericenter (Fig. 2, right). Hence, the pericentric collision line (black) limits the border of the resonance in Fig. 6 (top panel). Libration in the resonance with center $\phi^{\star}_{12} = 0$ is only possible above this collision line which coincides with a chaotic (yellow) strip separating the regular resonant and non-resonant regions.

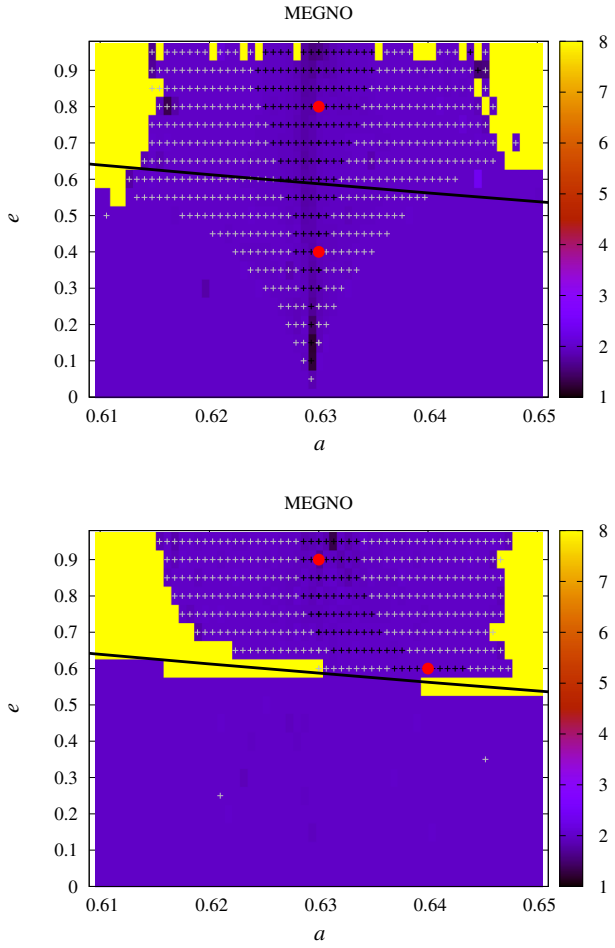

Fig. 5 Stability map showing regular (*blue*) and chaotic (*yellow*) regions for retrograde 2/1 resonance with $\phi_{21}^{\star} = 0$ (*top*) or $\phi_{21}^{\star} = 180^{\circ}$ (*low*) when $\mu = 0.001$. The *symbol plus* marks initial conditions such that $\phi_{21}^{\star}$ librates around 0 (*top*) or 180° (*low*) with amplitude less than 50° (*black* +), less than 300° (*gray* +). The apocentric collision line is shown in *black*. The initial conditions corresponding to orbits in Fig. 1 (*left*) are marked with *red circles on the top panel*, while those corresponding to orbits in Fig. 1 (*right*) are marked with *red circles* on the *low panel*. The 2 *gray plus symbols* below the apocentric collision line (*low panel*) correspond to non-resonant orbits that are wrongly associated with large amplitude libration due to output sampling. (Color figure online)

5 Discussion

In this article, we extended our work on the stability of retrograde configurations and the nature of retrograde resonance in the framework of the planar circular restricted three-body problem (CR3BP) consisting of a star, planet and test particle (Morais and Giuppone 2012; Morais and Namouni 2013).

We obtained the stability boundary for retrograde configurations in the low mass (planetary) regime and showed that it is located within the planet's Hill's radius and that there is an asymmetry between the inner and outer boundaries. In contrast, the stability boundary for

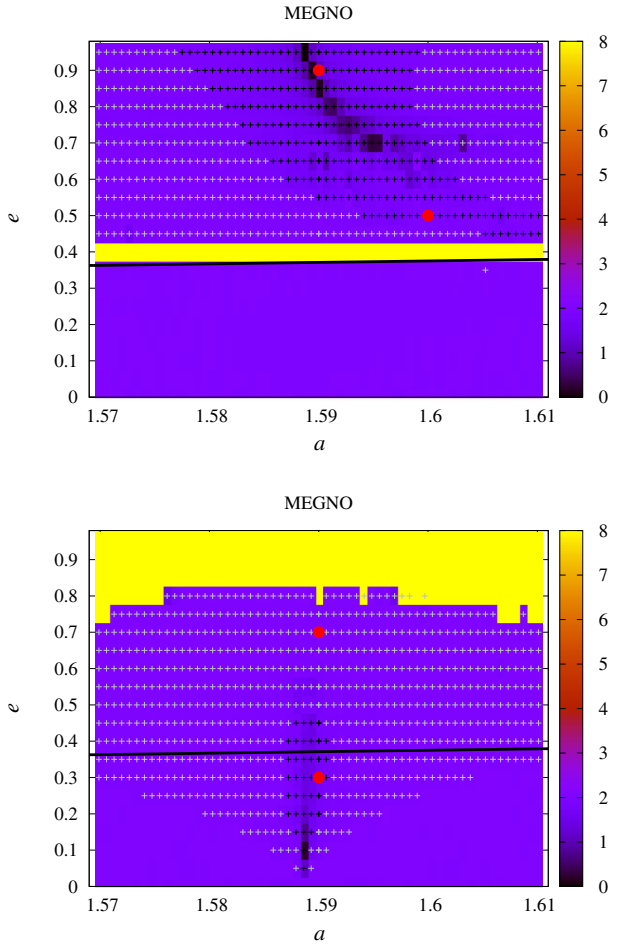

Fig. 6 Stability map showing regular (*blue*) and chaotic (*yellow*) regions for retrograde 1/2 resonance with $\phi_{12}^{\star} = 0$ (*top*) or $\phi_{12}^{\star} = 180^{\circ}$ (*low*) when $\mu = 0.001$. The *symbol plus marks* initial conditions such that $\phi_{12}^{\star}$ librates around 0 (*top*) or 180° (*low*) with amplitude less than 50° (*black* +), less than 300° (*gray* +). The pericentric collision line is shown in *black*. The initial conditions corresponding to orbits in Fig. 2 (*left*) are marked with *red circles on the top panel*, while those corresponding to orbits in Fig. 2 (*right*) are marked with *red circles on the low panel*. The *gray* + symbol just below the pericentric collision line (*top panel*) correspond to a non-resonant orbit that is wrongly associated with large amplitude libration due to output sampling. (Color figure online)

prograde configurations is located at several planet's Hill's radius and is approximated by Wisdom's criterion of first-order orbital resonances' overlap. These results help understand the numerical simulations in Namouni and Morais (2015) that showed that smooth migration capture in the 1/1 (co-orbital) resonance occurs with probability 1 for planar retrograde configurations but with probability 0 for planar prograde configurations. We leave further investigation of this capture mechanism for a future publication

We obtained stability maps in a grid of semi-major axis versus eccentricity for the 2/1 and 1/2 retrograde resonances and showed the regions of libration of the critical arguments. The resonance borders are delimited by the collision separatrix with the planet whose location

depends on the geometry of the resonance configuration and does not necessarily occur at pericenter (apocenter) for outer (inner) resonances. In the configurations where collision is possible at apocenter or pericenter our results agree with a study of prograde third- and fourth-order resonances in the planar CR3BP by Érdi et al. (2012).

Stability studies of individual retrograde resonances are important to understand the origin of the Solar System small bodies in retrograde resonance with Jupiter and Saturn identified by Morais and Namouni (2013). Retrograde resonances may also exist in extrasolar systems (Gayon and Bois 2008; Gayon-Markt and Bois 2009; Goździewski et al. 2013) although no cases have yet been confirmed due to the difficulty in measuring relative inclinations.

Acknowledgments We would like to acknowledge the assistance of Nelson Callegari Jr. with computational resources.

References

Cincotta PM, Simó C (2000) Simple tools to study global dynamics in non-axisymmetric galactic potentials—I. A&AS 147:205–228. doi:10.1051/aas:2000108

Eberle J, Cuntz M (2010) On the reality of the suggested planet in the ν Octantis system. Astrophys J 721:L168–L171. doi:10.1088/2041-8205/721/2/L168

Érdi B, Rajnai R, Sándor Z, Forgács-Dajka E (2012) Stability of higher order resonances in the restricted three-body problem. Celest Mech Dyn Astron 113:95–112. doi:10.1007/s10569-012-9420-4

Gayon J, Bois E (2008) Are retrograde resonances possible in multi-planet systems? Astron Astrophys 482:665–672. doi:10.1051/0004-6361:20078460

Gayon-Markt J, Bois E (2009) On fitting planetary systems in counter-revolving configurations. Mon Not R Astron Soc 399:L137–L140. doi:10.1111/j.1745-3933.2009.00740.x

Goździewski K (2003) Stability of the HD 12661 planetary system. Astron Astrophys 398:1151–1161. doi:10.1051/0004-6361:20021713

Goździewski K, Słonina M, Migaszewski C, Rozenkiewicz A (2013) Testing a hypothesis of the ν Octantis planetary system. Mon Not R Astron Soc 430:533–545. doi:10.1093/mnras/sts652

Morais MHM, Correia ACM (2012) Precession due to a close binary system: an alternative explanation for ν-Octantis? Mon Not R Astron Soc 419:3447–3456. doi:10.1111/j.1365-2966.2011.19986.x

Morais MHM, Giuppone CA (2012) Stability of prograde and retrograde planets in circular binary systems. Mon Not R Astron Soc 424:52–64. doi:10.1111/j.1365-2966.2012.21151.x

Morais MHM, Namouni F (2013) Asteroids in retrograde resonance with Jupiter and Saturn. Mon Not R Astron Soc 436:L30–L34. doi:10.1093/mnrasl/slt106

Morais MHM, Namouni F (2013) Retrograde resonance in the planar three-body problem. Celest Mech Dyn Astron 117:405–421. doi:10.1007/s10569-013-9519-2

Murray CD, Dermott SF (1999) Solar system dynamics. Cambridge University Press, Cambridge

Namouni F, Morais MHM (2015) Resonance capture at arbitrary inclination. Mon Not R Astron Soc 446:1998–2009. doi:10.1093/mnras/stu2199

Perets HB, Kouwenhoven MBN (2012) On the origin of planets at very wide orbits from the recapture of free floating planets. Astrophys J 750:83. doi:10.1088/0004-637X/750/1/83

Ramm DJ, Pourbaix D, Hearnshaw JB, Komonjinda S (2009) Spectroscopic orbits for K giants β Reticuli and ν Octantis: what is causing a low-amplitude radial velocity resonant perturbation in ν Oct? Mon Not R Astron Soc 394:1695–1710. doi:10.1111/j.1365-2966.2009.14459.x

Varvoglis H, Sgardeli V, Tsiganis K (2012) Interaction of free-floating planets with a star–planet pair. Celest Mech Dyn Astron 113:387–402. doi:10.1007/s10569-012-9429-8

Wisdom J (1980) The resonance overlap criterion and the onset of stochastic behavior in the restricted three-body problem. Astron J 85:1122–1133. doi:10.1086/112778